Diffuse charge dynamics in ionic thermoelectrochemical systems

Robert F. Stout and Aditya S. Khair*
Department of Chemical Engineering, Carnegie Mellon University, Pittsburgh, Pennsylvania 15213, USA
(Received 26 May 2017; published 7 August 2017)

Thermoelectrics are increasingly being studied as promising electrical generators in the ongoing search for alternative energy sources. In particular, recent experimental work has examined thermoelectric materials containing ionic charge carriers; however, the majority of mathematical modeling has been focused on their steady-state behavior. Here, we determine the time scales over which the diffuse charge dynamics in ionic thermoelectrochemical systems occur by analyzing the simplest model thermoelectric cell: a binary electrolyte between two parallel, blocking electrodes. We consider the application of a temperature gradient across the device while the electrodes remain electrically isolated from each other. This results in a net voltage, called the thermovoltage, via the Seebeck effect. At the same time, the Soret effect results in migration of the ions toward the cold electrode. The charge dynamics are described mathematically by the Poisson-Nernst-Planck equations for dilute solutions, in which the ion flux is driven by electromigration, Brownian diffusion, and thermal diffusion under a temperature gradient. The temperature evolves according to the heat equation. This nonlinear set of equations is linearized in the (experimentally relevant) limit of a "weak" temperature gradient. From this, we show that the time scale on which the thermovoltage develops is the Debye time, $1/D\kappa^2$, where D is the Brownian diffusion coefficient of both ion species, and κ^{-1} is the Debye length. However, the concentration gradient due to the Soret effect develops on the bulk diffusion time, L^2/D, where L is the distance between the electrodes. For thin diffuse layers, which is the condition under which most real devices operate, the Debye time is orders of magnitude less than the diffusion time. Therefore, rather surprisingly, the majority of ion motion occurs after the steady thermovoltage has developed. Moreover, the dynamics are independent of the thermal diffusion coefficients, which simply set the magnitude of the steady-state thermovoltage.

DOI: 10.1103/PhysRevE.96.022604

I. INTRODUCTION

The thermoelectric effect is the generation of a voltage across an electrically conducting material in response to an applied temperature gradient. When subjected to a temperature gradient, charge carriers will tend to migrate toward colder regions of the material [1], but they have differing thermal diffusion coefficients, thereby generating a "thermovoltage," V_T. This is analogous to the "diffusion potential" generated under an applied concentration gradient of charge carriers [2]. The thermovoltage is related to the temperature difference across the material, ΔT, by the Seebeck coefficient, Se, or thermopower,

$$V_T = -\mathrm{Se}\Delta T, \tag{1}$$

where the negative sign is by definition such that the lower temperature corresponds to a higher potential. The ability of a thermoelectric material to convert thermal energy into electrical energy is characterized by the figure of merit, $ZT = \mathrm{Se}^2\sigma T/\lambda$, where σ is the electrical conductivity and λ is the thermal conductivity [3]. Physically, this represents the electrical energy stored relative to the thermal energy dissipated via conduction. Traditional thermoelectric devices utilize inorganic semiconducting materials, which contain electronic charge carriers, resulting in $ZT \approx 0.1$–1, while nanostructured devices have been fabricated with $ZT \approx 2$–3.5 [4–6], achieved by having large electrical conductivities, $O(10^3\mathrm{S/cm})$, at room temperature, and Seebeck coefficients of $O(100\,\mu\mathrm{V/K})$ [6,7]. However, this still places their efficiency below that of other heat engines [4]. Moreover, these inorganic thermoelectrics are usually composed of rare, expensive, and sometimes toxic materials [8].

Due to these drawbacks, there has been recent interest in "soft" thermoelectric materials containing ionic charge carriers, such as ionic liquids [9–11], nonaqueous organic electrolytes [12], and mixed ionic-electronic conducting polymers [13–17]. Although these come with a reduction in electrical conductivity compared to semiconductor-based thermoelectrics, they can be competitive due to having much larger Seebeck coefficients, on the order of mV/K [12,15–17]. This enables such materials to store more charge [17], and it provides a pathway for designing devices that have figures of merit comparable to semiconductor-based devices. In addition, the materials used tend to be much cheaper to process and less toxic, making them good candidates for wearable devices and mass production [8].

For example, Zhao *et al.* [17] utilized polyethylene oxide with anionic end groups and sodium ions as the counterions to obtain a Seebeck coefficient of 11.1 mV/K. Chang *et al.* [15] used polymeric ethylenedioxythiophene (PEDOT) and polystyrenesulfonate (PSS) doped with silver ions and achieved Se = 0.1 mV/K with $ZT = 0.13$, stable over $O(10^3\,\mathrm{s})$, compared to the undoped material, which exhibited a decay in Se over $O(100\,\mathrm{s})$. Kim *et al.* [16] use a PSS-based thermoelectric generator to achieve an ionic Seebeck coefficient of 8 mV/K and $ZT = 0.4$. A nonaqueous solution of tetrabutylammonium nitrate in dodecanol was reported to have Se = 7 mV/K by Bonetti *et al.* [12].

Given the growing interest in and improvement of these devices, an investigation of the dynamics of diffuse ionic charge carriers in thermoelectric materials is warranted.

*Corresponding author: akhair@andrew.cmu.edu

However, mathematical modeling for even the simplest case of a binary electrolyte has not included an analysis of the charging dynamics, and instead considers only the steady-state thermovoltage and ion distributions across a device [18–20]. At steady state, in an electroneutral binary electrolyte, the Seebeck coefficient is $\mathrm{Se}_E = k_B(\alpha_+ - \alpha_-)/e$ [20], where k_B is Boltzmann's constant, e is the elementary charge, and the subscript E denotes the steady-state electroneutral solution value. The quantities α_+ and α_- are the reduced Soret coefficients, which are related to the ratios of the thermal diffusion coefficients to the Brownian diffusion coefficients of the cation (+) and anion (−), respectively. For the similar problem of a suddenly applied voltage at a constant, uniform temperature, the relevant time scale for the charging of the Debye, or diffuse, screening layers of ionic charge adjacent to the electrodes is the RC time, $L/D\kappa$, where L is the distance between electrodes, $1/\kappa$ is the Debye length, and D is the Brownian diffusion coefficient of the ions [21]. However, it is not clear what the time scale would be for a suddenly applied temperature gradient, since the ions undergo both Brownian and thermal diffusion. A central goal of the present paper is to address this point.

Therefore, we systematically investigate the charge dynamics of a prototypical ionic thermoelectrochemical cell subjected to a suddenly applied temperature gradient between two parallel, perfectly blocking electrodes. We find that, for "weak" applied temperature gradients (where "weak" will be defined precisely in what follows), the Debye time, $1/D\kappa^2$, is the relevant time scale for development of the thermovoltage and charging of the diffuse layers, whereas the diffusion time, L^2/D, is the time scale of bulk diffusion of neutral salt across the cell. In Sec. II, we formulate the mathematical problem and obtain the time scales for charge, salt, and thermovoltage evolution. In Sec. III, we examine the time evolution of the profiles for these quantities across the cell. In Sec. IV, we offer some concluding remarks.

II. PROBLEM FORMULATION

Consider two parallel electrodes a distance $2L$ apart that are not connected via an external circuit (Fig. 1). The space between the electrodes is occupied by a fully dissociated binary electrolyte solution with positive ion number density n_+ and negative ion number density n_-. The cations (+) and anions (−) have equal charge number, z, and equal Brownian diffusion coefficients, D, but differing thermal diffusion coefficients, $D_{T,i}$, such that their reduced Soret coefficients are α_+ and α_-, respectively, and $\alpha_+ \neq \alpha_-$. Initially, at time $t < 0$, the system is in thermal equilibrium at a constant, uniform temperature T_0, with uniform ion number densities $n_{+,0}$ and $n_{-,0}$. At time $t \geqslant 0$, the electrode at $x = +L$ (henceforth referred to as the hot electrode) is heated to a temperature $T_H > T_0$ while the electrode at $x = -L$ (the cold electrode) is maintained at the initial temperature T_0.

As the heat propagates through the cell, the ions migrate via the Soret effect toward the cold electrode [1,22], which is balanced by Brownian diffusion and electromigration via the induced electric field within the cell. The ions migrate at different rates according to their reduced Soret coefficients, $\alpha_i = T D_{T,i}/2D$. For example, in the simple salt KCl, the

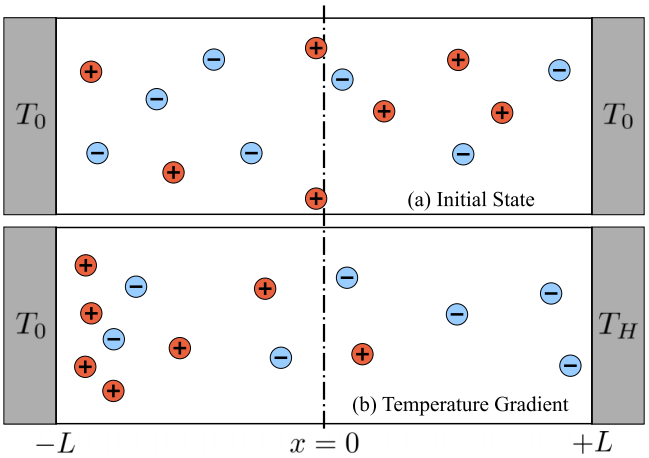

FIG. 1. Sketch of the model problem. The initial, isothermal state is depicted in (a); the charges are uniformly distributed. Upon heating the electrode at $x = +L$ to a temperature $T_H > T_0$, the charges migrate toward the colder regions of the cell, shown in (b). Two effects are depicted in (b): the concentration gradient and the regions of net charge near the electrodes.

Brownian diffusion coefficients are approximately equal [23] but the reduced Soret coefficients are $\alpha_+ = 0.5$ and $\alpha_- = 0.1$ [19]. This tendency to migrate at different rates results in a local electric field and hence a macroscopic voltage across the cell, termed the thermovoltage, which acts to ensure no net current.

Assuming the distance between the electrodes is much smaller than the other dimensions, which is reasonable considering devices often have separations on the order of millimeters [15–17], the dynamics of this system are governed by the one-dimensional ion conservation equation,

$$\frac{\partial n_\pm}{\partial t} = -\frac{\partial j_\pm}{\partial x}, \tag{2}$$

where t is time, and $j_\pm$ is the flux of the cations (+) or anions (−), given by [19]

$$j_\pm = -Dn_\pm\left(\frac{\partial \ln n_\pm}{\partial x} \pm \frac{ze}{k_B T}\frac{\partial \phi}{\partial x} + 2\alpha_\pm \frac{\partial \ln T}{\partial x}\right), \tag{3}$$

where e is the elementary charge, k_B is Boltzmann's constant, T is temperature, and ϕ is the electrostatic potential. Equation (3) therefore represents the sum of the Brownian-diffusive, electromigrative, and thermodiffusive fluxes of ions, respectively.

The electrostatic potential is governed by Poisson's equation,

$$-\frac{\partial}{\partial x}\left(\varepsilon\frac{\partial \phi}{\partial x}\right) = \rho = ez(n_+ - n_-), \tag{4}$$

where ε is the permittivity of the solution and ρ is the ionic charge density. Finally, the temperature evolves according to the heat equation,

$$\frac{\partial}{\partial t}(\eta C_p T) = \frac{\partial}{\partial x}\left(\lambda\frac{\partial T}{\partial x}\right), \tag{5}$$

where η is the density, C_p is the heat capacity per mass, and λ is the thermal conductivity of the solution.

These equations are supplemented with the following initial conditions specifying temperature, and the uniform ion

densities:

$$T(x,t<0)=T_0, \tag{6a}$$

$$n_\pm(x,t<0)=n_{\pm,0}. \tag{6b}$$

The boundary conditions specify no flux of ions and no electric field at the electrode surfaces, and the temperature applied to the electrodes:

$$j_\pm(x=+L,t\geqslant 0)=0, \tag{7a}$$

$$j_\pm(x=-L,t\geqslant 0)=0, \tag{7b}$$

$$\frac{\partial\phi}{\partial x}(x=\pm L,t\geqslant 0)=0, \tag{7c}$$

$$T(x=+L,t\geqslant 0)=T_H, \tag{7d}$$

$$T(x=-L,t\geqslant 0)=T_0. \tag{7e}$$

Equation (7c) arises from Gauss's law and the fact that there is no external circuit connected to either electrode through which they could develop a charge. Note that (7d) assumes the electrode is instantly heated from T_0 to T_H. The ultimate quantity of interest, the thermovoltage generated, is calculated from an integral of the resultant electrostatic potential gradient across the entire cell,

$$V_T=\int_{-L}^{+L}\frac{\partial\phi}{\partial x}dx=\phi(L,t)-\phi(-L,t). \tag{8}$$

A. Linear dynamics under weak temperature gradients

This mathematical problem (2)–(8) is impossible to solve exactly. Not only are there nonlinearities in the ion flux equations (3), but the physical properties (permittivity, diffusion coefficients, etc.) of the solution vary with temperature and hence with time and position. In general, mathematical expressions, or experimentally determined correlations, to approximate the temperature dependence of these properties would be necessary. To make progress, we assume that, after all transients have died out, the resulting temperature gradient $G_f=(T_H-T_0)/2L$ is small, such that $G_f\ll T_0/2L$. This condition can be expressed solely in terms of the temperatures involved as $\Delta T\ll T_0$, where $\Delta T=T_H-T_0$. Assuming a thermoelectric device is intended to operate at least at room temperature, $T_0\approx 300$ K, then $O(1$ K) temperature differences would readily suffice to meet this condition. Several devices operate in this regime [12,15–17]. Thus, defining a small parameter $\delta=G_f 2L/T_0=\Delta T/T_0\ll 1$, we can express all unknowns as perturbations to their initial state by a small temperature gradient. Hence for a general quantity, $f=f_0+\delta f_1$, where f_0 is the initial state and f_1 is the perturbed contribution due to the temperature gradient. The resulting $O(1)$ problem is merely the initial state of the system prior to applying a temperature gradient, and the $O(\delta)$ problem becomes

$$\frac{\partial n_{\pm,1}}{\partial t}=-\frac{\partial j_{\pm,1}}{\partial x}, \tag{9a}$$

$$j_{\pm,1}=-D_0\left(\frac{\partial n_{\pm,1}}{\partial x}\pm\frac{zen_{\pm,0}}{k_BT_0}\frac{\partial\phi_1}{\partial x}+\frac{2\alpha_{\pm,0}n_{\pm,0}}{T_0}\frac{\partial T_1}{\partial x}\right), \tag{9b}$$

$$\frac{\partial^2\phi_1}{\partial x^2}=-\frac{\rho_1}{\varepsilon_0}=-\frac{ez}{\varepsilon_0}(n_{+,1}-n_{-,1}), \tag{9c}$$

$$\frac{\partial T_1}{\partial t}=\frac{\lambda_0}{\eta_0 C_{p,0}}\frac{\partial^2 T_1}{\partial x^2}, \tag{9d}$$

where to obtain (9d) it is assumed that the heat capacity and density do not change appreciably with temperature such that the ratios $C_{p,1}/C_{p,0}$ and η_1/η_0 are negligible. This is a reasonable assumption for dilute aqueous electrolytes [23]. The initial and boundary conditions for the $O(\delta)$ problem are

$$n_{\pm,1}(x,t<0)=0, \tag{10a}$$

$$T_1(x,t<0)=0, \tag{10b}$$

$$j_{\pm,1}(x=+L,t\geqslant 0)=0, \tag{10c}$$

$$j_{\pm,1}(x=-L,t\geqslant 0)=0, \tag{10d}$$

$$\frac{\partial\phi_1}{\partial x}(x=\pm L,t\geqslant 0)=0, \tag{10e}$$

$$T_1(x=+L,t\geqslant 0)=T_0, \tag{10f}$$

$$T_1(x=-L,t\geqslant 0)=0, \tag{10g}$$

and the thermovoltage is obtained from (8) as

$$V_T=\delta\int_{-L}^{+L}\frac{\partial\phi_1}{\partial x}dx=\delta[\phi_1(L,t)-\phi_1(-L,t)]. \tag{11}$$

Next, we eliminate temperature as an unknown quantity by assuming that the heat diffusivity is much greater than both ion diffusion coefficients, i.e., $\lambda_0/\eta_0 C_{p,0}\gg D_0$ and $\lambda_0/\eta_0 C_{p,0}\gg T_0 D_{T,0}$. That is, we assume the temperature within the electrolyte responds instantaneously to variations in the electrode temperature, compared to the response of the ions. This assumption is valid for aqueous solutions of electrolytes, where the ratio $\lambda/\eta C_p D\approx 100$ [23] and $\alpha_i\sim O(1)$ [19]. For thermoelectric devices that use large, nonaqueous, or organic charge carriers, this ratio will be much greater than unity due to a smaller Brownian-diffusion coefficient [24] but only a slightly reduced thermal diffusivity [25]. Therefore, compared to the relatively slow diffusion of ions, the heat diffuses rapidly through the cell, and the temperature has the quasisteady linear profile

$$T(x,t)=T_0+G(t)(x+L), \tag{12}$$

where $G(t)=[T_H(t)-T_0]/2L$ is the time-dependent temperature gradient, reflecting the heating of the hot electrode. We now assume that the hot electrode achieves its final temperature instantaneously, and we replace $G(t)$ with G_f. To eliminate T_1 from (9b), we express the left-hand side of (12) as a perturbation expansion and obtain $\partial T_1/\partial x=G_f/\delta=T_0/2L$. The linearized ion flux is thus

$$j_{\pm,1}=-D_0\left(\frac{\partial n_{\pm,1}}{\partial x}\pm\frac{zen_{\pm,0}}{k_BT_0}\frac{\partial\phi_1}{\partial x}+\frac{\alpha_{\pm,0}n_{\pm,0}}{L}\right), \tag{13}$$

and the thermodiffusive contribution has been reduced to a constant at this order, $-D_0\alpha_{\pm,0}n_{\pm,0}/L$.

Next, we define

$$c=\frac{n_++n_-}{2z}, \tag{14a}$$

$$\rho_c=\frac{n_+-n_-}{2z}, \tag{14b}$$

such that c represents the neutral salt concentration and $e\rho_c$ represents a corresponding charge density. Substituting these

definitions into (9) and (13) yields

$$\frac{\partial c_1}{\partial t} = D\frac{\partial^2 c_1}{\partial x^2}, \tag{15a}$$

$$\frac{\partial \rho_{c,1}}{\partial t} = D\frac{\partial^2 \rho_{c,1}}{\partial x^2} - D\kappa^2 \rho_{c,1}, \tag{15b}$$

$$\frac{\partial^2 \phi_1}{\partial x^2} = -\frac{2ez^2}{\varepsilon_0}\rho_{c,1}, \tag{15c}$$

where $1/\kappa = \sqrt{\varepsilon_0 k_B T_0/2e^2 z^3 c_0}$ is the Debye length in terms of the initial state, prior to applying a temperature gradient. The initial and boundary conditions (10a)–(10d) become

$$c_1(x,t<0) = 0, \tag{16a}$$

$$\rho_{c,1}(x,t<0) = 0, \tag{16b}$$

$$\frac{\partial c_1}{\partial x}(\pm L,t) = -\frac{c_0\alpha_m}{L}, \tag{16c}$$

$$\frac{\partial \rho_{c,1}}{\partial x}(\pm L,t) = -\frac{c_0\alpha_d}{L}, \tag{16d}$$

where $\alpha_m = (\alpha_{+,0} + \alpha_{-,0})/2$ and $\alpha_d = (\alpha_{+,0} - \alpha_{-,0})/2$, and we have used (10e) to eliminate the electrostatic potential gradient. Note that, at least to first order in the applied gradient, all thermal dependence is found in the boundary conditions (16c) and (16d) through the reduced Soret coefficients. Physically, this means, as we will see, that changing the Soret coefficients alters only the magnitude of the charge density, concentration, and thermovoltage at any point in time; the charging dynamics are unaffected. That is, surprisingly, we expect the time it takes to reach a steady state to be independent of the thermal diffusion of the ions.

We now introduce Laplace transforms, defined by

$$\hat{f}(x,s) = \int_0^\infty e^{-st} f(x,t)dt, \tag{17}$$

where s is the Laplace frequency. The governing equations are thus transformed to

$$\frac{d^2\hat{c}_1}{dx^2} = r^2\hat{c}_1, \tag{18a}$$

$$\frac{d^2\hat{\rho}_{c,1}}{dx^2} = k^2\hat{\rho}_{c,1}, \tag{18b}$$

$$\frac{d^2\hat{\phi}_1}{dx^2} = -\frac{2ez^2}{\varepsilon_0}\hat{\rho}_{c,1}, \tag{18c}$$

where

$$k^2 = \frac{s}{D} + \kappa^2 \quad \text{and} \quad r^2 = \frac{s}{D},$$

with boundary conditions

$$\frac{\partial \hat{c}_1}{\partial x}(\pm L,s) = -\frac{c_0\alpha_m}{Ls}, \tag{19a}$$

$$\frac{\partial \hat{\rho}_{c,1}}{\partial x}(\pm L,s) = -\frac{c_0\alpha_d}{Ls}. \tag{19b}$$

These equations are readily solved, yielding

$$\hat{c}_1(x,s) = -\frac{c_0\alpha_m}{rLs}\left(\frac{\sinh(rx)}{\cosh(rL)}\right), \tag{20a}$$

$$\hat{\rho}_{c,1}(x,s) = -\frac{c_0\alpha_d}{kLs}\left(\frac{\sinh(kx)}{\cosh(kL)}\right), \tag{20b}$$

$$\hat{\phi}_1(x,s) = -\frac{kT_0\alpha_d\kappa^2}{ezk^2s}\left(\frac{x}{L} - \frac{\sinh(kx)}{kL\cosh(kL)}\right). \tag{20c}$$

The Laplace transform of (11) yields $\hat{V}(s) = 2\delta\hat{\phi}_1(L,s)$; therefore, the Laplace transform of the thermovoltage is given by

$$\hat{V}(s) = -\frac{2k\Delta T\alpha_d\kappa^2}{ezk^2s}\left(1 - \frac{\tanh(kL)}{kL}\right). \tag{21}$$

The first term in both (20c) and (21) is due to the linear electrostatic potential drop across the bulk, electroneutral solution. In this region, the electric field that results from the unequal thermomigration of the ion species is uniform. However, near the electrodes, diffuse layers with nonzero net charge develop and screen this electric field on the length scale $1/\kappa$, described by the second term in (20c) and (21).

B. Determining time scales for thermoelectric charging

To determine the time scales for neutral salt diffusion, charge separation, and thermovoltage evolution, we evaluate (20) at the cold electrode ($x = -L$). However, it is difficult to obtain physical insights into the dynamics from direct analytic inversion of the resulting equations. Therefore, we consider the limit of long times, $t \to \infty$, by taking the limit $s \to 0$. By expressing (20) and (21) as Taylor series about $s = 0$, we can obtain expressions of the form $(1/s)/(1+\tau s)$, which has an inverse Laplace transform of $(1 - e^{-t/\tau})$, where τ is the time scale that we seek. Doing so, we find

$$c_1(-L,t) \sim c_0\alpha_m(1 - e^{-t/\tau_c}), \tag{22a}$$

$$\rho_{c,1}(-L,t) \sim \frac{c_0\alpha_d\tanh(\kappa L)}{\kappa L}(1 - e^{-t/\tau_\rho}), \tag{22b}$$

$$V_T(t) \sim -\frac{2k_B\Delta T\alpha_d}{ez}\left(1 - \frac{\tanh(\kappa L)}{\kappa L}\right)(1 - e^{-t/\tau_\phi}), \tag{22c}$$

where

$$\tau_c = \frac{L^2}{3D}, \tag{23a}$$

$$\tau_\rho = \frac{1}{2D\kappa^2}\left(1 - \frac{2\kappa L}{\sinh(2\kappa L)}\right), \tag{23b}$$

$$\tau_\phi = \frac{1}{2D\kappa^2}\frac{3\tanh(\kappa L) + \kappa L[\tanh^2(\kappa L) - 3]}{\tanh(\kappa L) - \kappa L} \tag{23c}$$

are the time scales associated with diffusion of neutral salt, diffuse layer charging, and thermovoltage evolution, respectively.

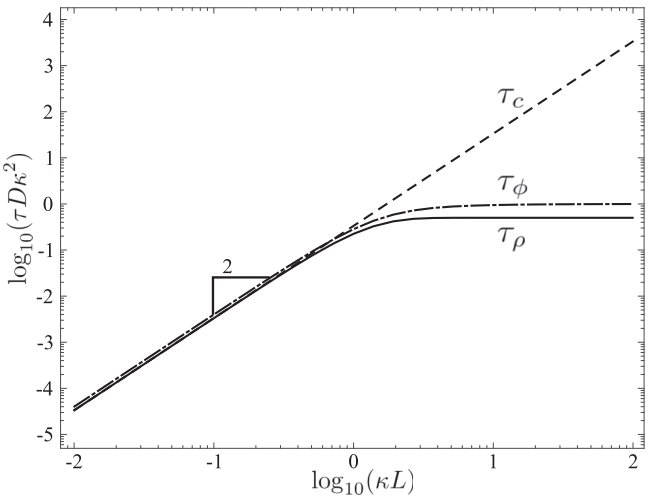

FIG. 2. Dimensionless time scales for charge density, τ_ρ (solid), and salt concentration, τ_c (dashed), at the cold electrode (the hot electrode exhibits identical time scales) as well as voltage, τ_ϕ (dot-dashed), vs κL. For $\kappa L \ll 1$, all time scales increase with a slope of 2. However, for $\kappa L \gg 1$, the charge density and voltage time scales reach a constant value of $1/2$ and 1, respectively, but the concentration time scale continues to increase at the same rate.

We see in (23) that the time scales for charge density and thermovoltage are both functions of κL but are proportional to the Debye time, $1/D\kappa^2$. In fact, for very thin diffuse layers, $\kappa L \to \infty$, $\tau_\rho \sim 1/2D\kappa^2$, and $\tau_\phi \sim 1/D\kappa^2$. This contrasts with the salt diffusion time scale, which is proportional to the bulk diffusion time, L^2/D, and is therefore independent of concentration and much longer than the Debye time for thin diffuse layers.

In Fig. 2, we compare the time scales (normalized by $1/D\kappa^2$) as a function of κL. For $\kappa L \ll 1$, or thick diffuse layers, all time scales are proportional to $(\kappa L)^2$ and hence diffuse charge, salt concentration, and voltage all evolve on essentially the same time scale, i.e., the diffusion time. For $\kappa L \gg 1$, or thin diffuse layers, the charge and voltage time scales achieve the limiting values mentioned above while the salt diffusion time scale continues to increase as $(\kappa L)^2$. This suggests that the salt concentration profile evolves much more slowly than the charging of the diffuse layers and the thermovoltage evolution for thin diffuse layers, which is the regime in which many devices operate [12,15–17].

Moreover, we see in Eq. (22c) that for thin diffuse layers, we recover the known steady-state Seebeck coefficient for an electroneutral solution, $-V_T(t \to \infty)/\Delta T = 2k_B\alpha_d/ez = \mathrm{Se}_E$ [20]. For finite κL, the Seebeck coefficient is reduced by $\mathrm{Se}_E \tanh(\kappa L)/\kappa L$ due to screening of the induced electric field by the nonzero net charge and incomplete charge separation due to overlapping diffuse layers. As the diffuse layer shrinks, and hence the regions of nonzero net charge shrink, the thermovoltage increases to the maximum value predicted for an electroneutral solution.

In Fig. 3, we plot the salt concentration and charge density at the cold electrode, calculated from the long-time solutions (22) and numerical inversion [26] of (20) versus time for several values of κL. Note that the concentration in Fig. 3(a) is the perturbed concentration relative to the uniform initial concentration. The positive perturbed concentration is the expected result of the Soret effect, namely that both ion species will be thermally induced to migrate toward the cold electrode. Further, as κL increases, it takes longer to reach the steady-state value, as predicted by the time scales (23) and Fig. 2.

For positive values of α_d, which corresponds to $\alpha_+ > \alpha_-$, the cations undergo faster thermal migration than the anions. This results in the positive diffuse charge at the cold electrode predicted in Fig. 3(b). Recall that we have assumed that both ion species have equal Brownian-diffusion coefficients. As κL increases, the amount of charge stored in the diffuse layer decreases and the equilibrium state is essentially achieved progressively closer to $t = 1/(2D\kappa^2)$, as indicated by the dashed vertical line in Fig. 3(b).

In Fig. 3(c), we plot the time-dependent Seebeck coefficient $\mathrm{Se}(t) = -V_T(t)/\Delta T$ versus time. Surprisingly, the long-time solution (22c) agrees well with the numerical inversion even at short times. The steady-state Seebeck coefficient increases with increasing κL, due to the shrinking diffuse layers as discussed previously. This indicates that in designing thermoelectric devices, it is advantageous to have the electrode separation much larger than the Debye length to achieve large Seebeck coefficients.

Other quantities, such as the total diffuse charge in the half of the cell near the cold electrode,

$$Q_T(t) = \int_{-L}^{0} \rho_c(x,t)dx, \tag{24}$$

and the total salt concentration in this same half,

$$C_T(t) = \int_{-L}^{0} c(x,t)dx, \tag{25}$$

also evolve with a long-time exponentially decaying transient to their steady state, but with different time scales. Using Laplace transforms on these definitions and substituting (20), we obtain

$$\hat{Q}_T(s) = \frac{c_0\alpha_d}{k^2Ls}[1 - \mathrm{sech}(kL)], \tag{26}$$

$$\hat{C}_T(s) = \frac{c_0\alpha_m}{r^2Ls}[1 - \mathrm{sech}(rL)]. \tag{27}$$

As before, direct inversion masks physical insights. Thus, in the long-time limit, we obtain

$$Q_T(t) \sim \frac{c_0\alpha_d}{\kappa^2 L}[1 - \mathrm{sech}(\kappa L)](1 - e^{-t/\tau_Q}), \tag{28a}$$

$$C_T(t) \sim \frac{c_0\alpha_m L}{2}(1 - e^{-t/\tau_C}), \tag{28b}$$

where

$$\tau_Q = \frac{1}{D\kappa^2}\left(1 - \frac{2\kappa L\cosh^2(\kappa L/2)}{\sinh(2\kappa L)}\right), \tag{29a}$$

$$\tau_C = \frac{5L^2}{12D} \tag{29b}$$

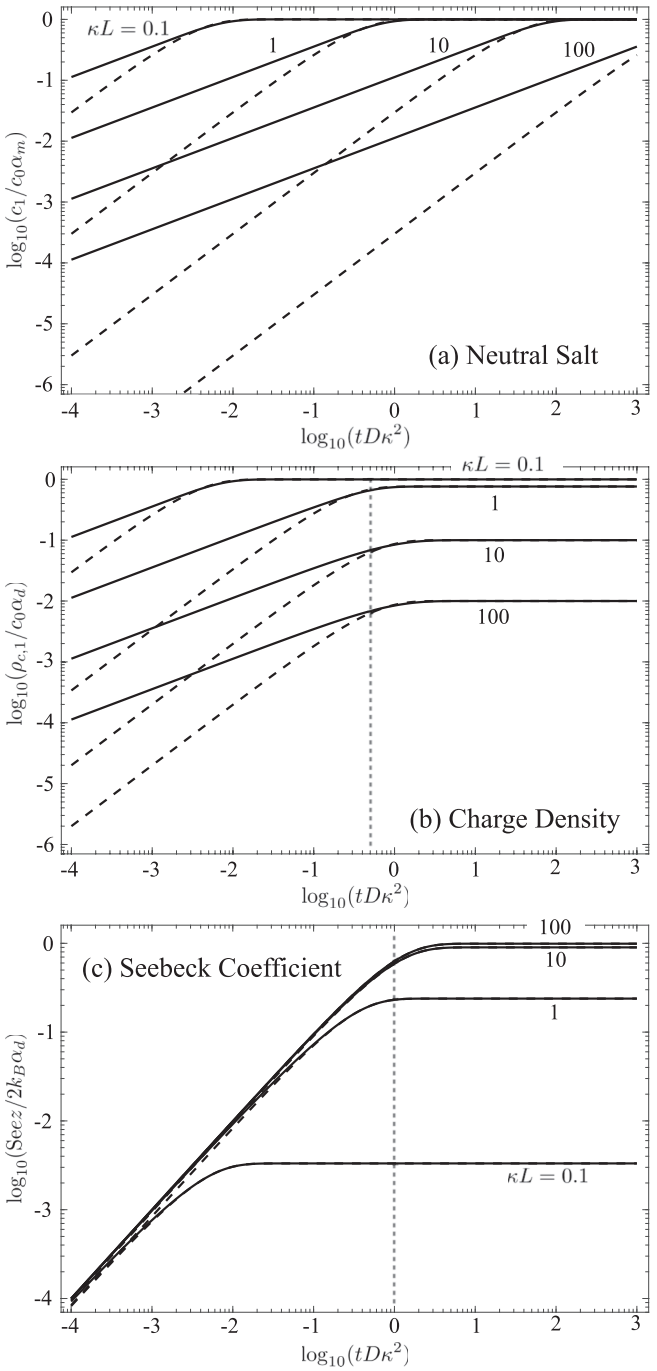

FIG. 3. Salt concentration (a) and charge density (b) at the cold electrode ($x = -L$) along with the Seebeck coefficient (c), $\mathrm{Se}(t) = -V(t)/\Delta T$, vs time at $\kappa L = 0.1$, 1, 10, and 100. Numerical Laplace transform inversions of (20) are shown as solid lines; dashed lines are the long-time solutions (22). The salt concentration increases monotonically, scaling as $\sqrt{t}$ at early times, until the steady-state level is reached. The time to achieve steady state increases as κL increases since the time scale for concentration evolution is L^2/D. The charge density also increases monotonically (again like $\sqrt{t}$ at early times) but achieves progressively lower charge densities at equilibrium for increasing κL. The Seebeck coefficient increases at approximately the same rate at early times (proportional to t), but it achieves progressively greater values, indicating larger thermovoltages, as κL increases. The vertical dashed line in (b) and (c) indicates the thin diffuse layer limit of the respective time scales.

are the time scales for total diffuse charge and total salt concentration. Clearly, the time scales have different κL dependency than those of the charge density, τ_ρ, and salt concentration, τ_c, at the cold electrode. However, for $\kappa L \gg 1$, the total diffuse charge time scale once again becomes the Debye time, $\tau_Q \sim 1/D\kappa^2$, and for $\kappa L \ll 1$, $\tau_Q \sim L^2/D$, which is identical to the time scales for the charge density at the electrodes, τ_ρ. Note also that the total diffuse charge decreases as κL increases. This reduction in nonzero net charge is what enables the Seebeck coefficient to increase with κL.

III. EVOLUTION OF CHARGE, SALT, AND ELECTROSTATIC POTENTIAL

We plot salt concentration, charge density, and electrostatic potential across the cell obtained via numerical inversion of (20). The quantities are plotted for $\kappa L = 5$ at times $tD\kappa^2 = 0.01$, 0.1, 1, and 1000, with the final time intended to capture the steady-state profile. In Fig. 4(a), we see that the salt slowly diffuses away from the hot electrode toward the cold electrode (for $\alpha_m > 0$). This diffusion begins near the electrodes, and, as the diffuse layers attain equilibrium, it extends to the bulk solution until the final linear profile is achieved.

As mentioned in the previous section, for $\alpha_d > 0$, the cations undergo stronger thermal migration than the anions, and hence the diffuse layer near the cold electrode obtains a net positive charge, while the diffuse layer near the hot electrode obtains a net negative charge, as shown in Fig. 4(b). Compared to the neutral salt, the diffuse layers are much nearer to their equilibrium state by $tD\kappa^2 \approx 1$. This suggests, surprisingly, that the majority of ion transport occurs *after* diffuse layer charging has occurred. This is similar to what has been predicted under a suddenly applied voltage [21], where there exists an initial salt depletion zone near the electrodes as the diffuse layers form for applied voltages greater than the thermal voltage, k_BT/e. These depletion zones are then filled on the diffusion time scale L^2/D. The difference here is that for an applied temperature difference, diffuse layers charge on the time scale $1/D\kappa^2$, whereas for an applied potential difference, the charging time scale is $L/D\kappa$, which is a factor of κL longer.

Finally, Fig. 4(c) shows that the electrostatic potential is linear in the bulk solution, indicating that a uniform induced electric field exists there. Near the electrodes, the electric field is screened by the nonzero net charge within the diffuse layers, leading to a nonlinear profile.

Note that both charge density and electrostatic potential share the same sign across the cell. This is distinctly different from the situation observed for an applied voltage, in which the electrostatic potential and charge density have opposite signs, and it is a consequence of the dynamics being driven by a temperature gradient. For instance, consider an electrolyte for which $\alpha_d > 0$: then, the net negative charge density at the hot electrode is driven toward the cold electrode by the electromigrative force [negative potentials in Fig. 4(c)] together with the thermal migration. This is balanced by the diffusive flux, which acts to equalize the salt concentration across the entire cell. Similarly, at the cold electrode (net charge is positive), the diffusive flux and electromigration

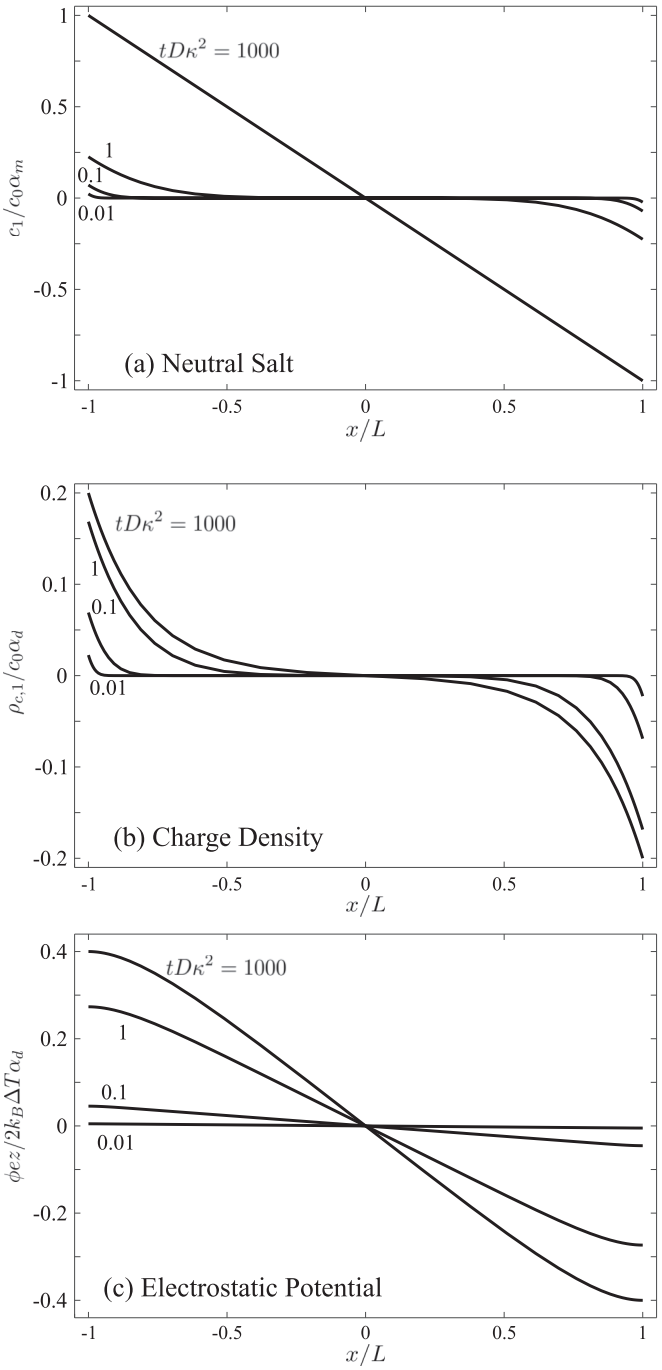

FIG. 4. Salt concentration (a), charge density (b), and electrostatic potential (c) across the cell at $tD\kappa^2 = 0.01$, 0.1, 1, and 1000 at $\kappa L = 5$. The heated electrode is located at $x/L = 1$ and the cold electrode is at $x/L = -1$. At steady state ($tD\kappa^2 \approx 1000$), the neutral salt has a linear profile and the electrostatic potential is linear only in the bulk solution, away from the net charge of the diffuse layers.

(toward the hot electrode) are balanced by the thermal migration (toward the cold electrode).

IV. CONCLUSIONS

We have provided a detailed derivation of the charging dynamics of an ionic thermoelectric system, starting from the fundamental ion transport equations for dilute electrolytes. We assumed a weak temperature gradient and defined a parameter to reflect this, $\delta = G_f 2L/T_0 \ll 1$, which sets a condition on the temperature difference: $\Delta T \ll T_0$. This condition can allow for rather large temperature differences provided the initial temperature of the device is appropriately chosen.

We predict that the thermovoltage and diffuse layers develop on the order of the Debye time, $1/D\kappa^2$, for thin diffuse layers, $\kappa L \gg 1$. In this regime, the Debye time is much shorter than both the diffusion time, L^2/D, over which the linear salt concentration profile develops, and the RC time, $L/D\kappa$, which is relevant for the related problem of a suddenly applied voltage in an isothermal system. As an example, consider that a 1 mM electrolyte solution has a Debye length of $1/\kappa \approx 10$ nm; then, assuming $D = 10^{-5}\,\mathrm{cm}^2/\mathrm{s}$ and $L = 1$ mm yields $\kappa L \approx 10^5$ and $L^2/D = 10^3$ s, while $1/D\kappa^2 \approx 10^{-7}$ s. This implies that the thermovoltage (and diffuse layers) develop extremely quickly as the device charges under a temperature gradient. However, salt diffusion due to the temperature gradient is much slower. Although the Debye length for devices used in experiments [15–17] can be difficult to calculate (as it depends on charge-carrier concentration, which can be uncertain), with electrode separations on the order of millimeters, we might reasonably assume that they operate with thin diffuse layers.

In this paper, we assumed the ions have equal Brownian diffusion coefficients, and relaxing this assumption would lead to different time scales; however, we expect to retain the same ordering of the time scales, i.e., steady thermovoltage develops more quickly than the steady concentration gradient. In experiments [15–17], one species is a large polymer molecule and it diffuses much more slowly (or is essentially fixed) relative to the other, hence unequal Brownian diffusion coefficients would be a more accurate representation of the physical systems. Furthermore, the time scales for salt diffusion, diffuse charge, and thermovoltage would necessarily have different limiting values for thin diffuse layers, but the magnitude of the thermovoltage might not be affected for weak temperature gradients, as only the Soret coefficients determine its magnitude. An alternative representation of real thermoelectric devices could be obtained by representing the electrolyte as a single ion conductor with a fixed "background" charge due to the nondiffusing species.

We had assumed the electrodes were not connected to each other, however the most practical application of a real device would be to have them connected via some external circuit in order to utilize the thermovoltage as it develops. In addition, most surfaces have some native charge, which we also neglected. Both of these conditions would mean replacing Eq. (10e) with one relating the time-dependent electric field to the surface charge density at the electrode surface. In principle, this surface charge density would also be temperature-dependent [27–29].

In addition, we have considered only the first-order effects of a weak temperature gradient. To this order, all thermal dependency exists only in the boundary conditions, and hence the Soret coefficients do not appear in the charging time scales. Perhaps beyond this weak gradient regime, the Soret coefficients play a greater role in the dynamics of the system, as opposed to merely determining the magnitude of the steady-state thermovoltage. One expected outcome is that

the Seebeck coefficient will depend on the magnitude of the temperature gradient, i.e., a "nonlinear" Seebeck coefficient. We will examine this and other issues raised in this section in future work.

ACKNOWLEDGMENT

The authors acknowledge NSF CAREER support under CBET-1350647.

[1] S. Duhr and D. Braun, Proc. Natl. Acad. Sci. USA **103**, 19678 (2006).
[2] D. C. Prieve, J. L. Anderson, J. P. Ebel, and M. E. Lowell, J. Fluid Mech. **148**, 247 (1984).
[3] H. S. Kim, W. Liu, G. Chen, C. W. Chu, and Z. Ren, Proc. Natl. Acad. Sci. USA **112**, 8205 (2015).
[4] C. B. Vining, Nat. Mater. **8**, 83 (2009).
[5] L. E. Bell, Science **321**, 1457 (2008).
[6] A. P. Gonçalves, E. B. Lopes, E. Alves, N. P. Barradas, N. Franco, O. Rouleau, and C. Godart, in *Properties and Applications of Thermoelectric Materials*, edited by V. Zlatic and A. C. Hewson (Springer, Dordrecht, The Netherlands, 2009).
[7] W. Fulkerson, J. P. Moore, R. K. Williams, R. S. Graves, and D. L. McElroy, Phys. Rev. **167**, 765 (1968).
[8] Y. He, T. Day, T. Zhang, H. Liu, X. Shi, L. Chen, and G. J. Snyder, Adv. Mater. **26**, 3974 (2014).
[9] H. Keppner, S. Uhl, E. Laux, L. Jeandupeux, J. Tschanz, and T. Journot, Mater. Today: Proc. **2**, 680 (2015).
[10] M. Bonetti, S. Nakamae, B. T. Huang, T. J. Salez, C. Wiertel-Gasquet, and M. Roger, J. Chem. Phys. **142**, 244708 (2015).
[11] T. J. Abraham, D. R. MacFarlane, and J. M. Pringle, Chem. Commun. **47**, 6260 (2011).
[12] M. Bonetti, S. Nakamae, M. Roger, and P. Guenoun, J. Chem. Phys. **134**, 114513 (2011).
[13] O. Bubnova, Z. U. Khan, A. Malti, S. Braun, M. Fahlman, M. Berggren, and X. Crispin, Nat. Mater. **10**, 429 (2011).
[14] Y. Xuan, X. Liu, S. Desbief, P. Leclère, M. Fahlman, R. Lazzaroni, M. Berggren, J. Cornil, D. Emin, and X. Crispin, Phys. Rev. B **82**, 115454 (2010).
[15] W. B. Chang, H. Fang, J. Liu, C. M. Evans, B. Russ, B. C. Popere, S. N. Patel, M. L. Chabinyc, and R. A. Segalman, ACS Macro Lett. **5**, 455 (2016).
[16] S. L. Kim, H. T. Lin, and C. Yu, Adv. Energy Mater. **6**, 1600546 (2016).
[17] D. Zhao, H. Wang, Z. U. Khan, J. C. Chen, R. Gabrielsson, M. P. Jonsson, M. Berggren, and X. Crispin, Energy Environ. Sci. **9**, 1450 (2016).
[18] G. Guthrie, J. N. Wilson, and V. Schomaker, J. Chem. Phys. **17**, 310 (1949).
[19] A. Majee and A. Würger, Phys. Rev. E **83**, 061403 (2011).
[20] S. A. Putnam and D. G. Cahill, Langmuir **21**, 5317 (2005).
[21] M. Z. Bazant, K. Thornton, and A. Ajdari, Phys. Rev. E **70**, 021506 (2004).
[22] R. Kita, S. Wiegand, and J. Luettmer-Strathmann, J. Chem. Phys. **121**, 3874 (2004).
[23] I. D. Zaytsev and G. G. Aseyev, in *Properties of Aqueous Solutions of Electrolytes*, translated by M. A. Lazarev and V. R. Sorochenko (CRC Press, Boca Raton, FL, 1992).
[24] J. L. Duda, Pure Appl. Chem. **57**, 1681 (1985).
[25] Q. Wei, M. Mukaida, K. Kirihara, and T. Ishida, ACS Macro Lett. **3**, 948 (2014).
[26] Numeric Laplace transform inversion was performed using the MATLAB function "INVLAP.m" by Mathworks.
[27] P. H. Tewari and A. B. Campbell, J. Colloid Interface Sci. **55**, 531 (1976).
[28] K. C. Akratopulu, C. Kordulis, and A. Lycourghiotis, J. Chem. Soc. Faraday Trans. **86**, 3437 (1990).
[29] M. Irshad, S. Mustafa, M. Waseem, K. H. Shah, and U. Rashid, J. Chem. Soc. Pak. **36**, 783 (2014).